

Observation of the symmetry-protected signature of 3-body interactions

Liudmila A. Zhukas^{1,*}, Qingfeng Wang^{1,2}, Or Katz^{1,3}, Christopher Monroe¹ and Iman Marvian¹

¹Duke Quantum Center, Departments of Electrical and Computer Engineering and Physics, Duke University, Durham, NC 27708

²Chemical Physics Program and Institute for Physical Science and Technology,
University of Maryland, College Park, Maryland, USA

³School of Applied and Engineering Physics, Cornell University, Ithaca, NY 14853.

Identifying and characterizing multi-body interactions in quantum processes remains a significant challenge. This is partly because 2-body interactions can produce an arbitrary time evolution, a fundamental fact often called the universality of 2-local gates in the context of quantum computing. However, when an unknown Hamiltonian respects a U(1) symmetry such as charge or particle number conservation, N-body interactions exhibit a distinct symmetry-protected signature known as the N-body phase, which fewer-body interactions cannot mimic. We develop and demonstrate an efficient technique for the detection of 3-body interactions despite the presence of unknown 2-body interactions. This technique, which takes advantage of GHZ states for phase estimation, requires probing the unitary evolution and measuring its determinant in a small subspace that scales linearly with the system size, making it an efficient approach.

Recent developments in quantum information science have revealed various new possibilities for generating and controlling multi-body interactions [1–5]. However, while such interactions can be a powerful resource in quantum computing, characterizing and identifying them also pose new challenges for standard approaches in this field. Therefore, developing new methods for detecting and learning such interactions is a timely and important goal for the field of quantum metrology and Hamiltonian learning [6–9]. Multi-body interactions appear in natural physical processes and may exist fundamentally, as seen in quantum chromodynamics, or emerge within effective theories when certain degrees of freedom or subspaces are integrated out [10]. Given the successful use of quantum metrology techniques for enhancing sensor signal-to-noise such as the detection of gravitational waves in the LIGO/VIRGO experiments [11, 12], it is natural to consider the use of such techniques for detecting other elusive physical phenomena such as 3-body interactions.

A no-go theorem– Do dynamics under 3-body interactions have any distinct signatures that cannot be reproduced by 2-body interactions, making them directly detectable? As an example, consider a system with n qubits interacting under a general Hamiltonian

$$H^{(3)}(t) = H^{(2)}(t) + \sum_{i < j < k} a_{ijk}^{(3)}(t) Z_i Z_j Z_k \quad : 0 \leq t \leq T, \quad (1)$$

where $H^{(2)}(t)$ can be decomposed as a sum of 2-local interactions, i.e., those that act non-trivially only on, at most, a pair of qubits, and Z_i denote Pauli Z operator on qubit i . As a concrete example, one may assume $H^{(2)}(t)$ contains a time-dependent XY interaction $X \otimes X + Y \otimes Y$ between nearest-neighbor qubits on a chain, as well as time-dependent single-qubit X and Z fields. The Hamiltonian $H^{(3)}$ may describe, e.g., a spin chain or the interaction between the internal degrees of freedom of particles that interact through a scattering

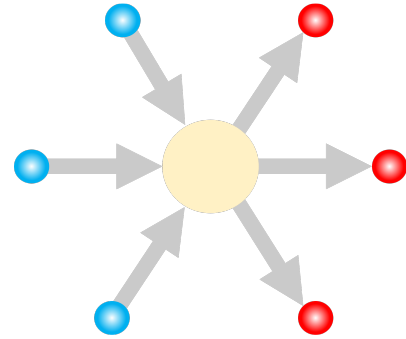


FIG. 1. **3-body interactions:** The Hamiltonian in Eq.(1) can be taken as a description of the interaction between the (blue) internal degrees of freedom of particles in a scattering process. By observing the (red) outputs of this process for different inputs, can we detect the presence of 3-body interactions $\sum a_{ijk}^{(3)}(t) Z_i Z_j Z_k$?

process (See Fig. 1).

Suppose we can prepare the system in arbitrary initial states which then evolve under the Hamiltonian $H^{(3)}(t)$ from time $t = 0$ to T . By performing such experiments can we obtain any information about the hypothetical 3-body term $\sum a_{ijk}^{(3)}(t) Z_i Z_j Z_k$? It turns out that the answer is negative.

Theorem: Consider a unitary process described by an unknown Hamiltonian $H^{(3)}(t)$ in the form of Eq.(1) for a fixed total time T . Suppose one can prepare arbitrary initial states and perform arbitrary measurements on the final state, and repeat this arbitrarily many times. Unless one has further information about the term $H^{(2)}(t)$ corresponding to the 2-body interactions in this Hamiltonian, it is impossible to detect the presence of 3-body interactions $\sum a_{ijk}^{(3)}(t) Z_i Z_j Z_k$, or to obtain any information about their strengths $a_{ijk}^{(3)}(t)$.

This no-go theorem is an immediate corollary of the universality of 2-qubit gates, which is one of the cornerstones of quantum computing [13, 14]: By choosing dif-

* Corresponding author: liudmila.zhukas@duke.edu

ferent input states and output measurements, the only information that can be obtained about the Hamiltonian $H^{(3)}$ is limited to what can be inferred from the unitary operator $V = \mathcal{T} \left\{ \exp \left(-i \int_0^T H^{(3)}(t) dt \right) \right\}$, where \mathcal{T} denotes the time-ordered integral and we take $\hbar = 1$. However, 2-body interactions in the Hamiltonian $H^{(3)}$ can synthesize any arbitrary unitary transformation. Therefore, adding three-body interactions does not extend the set of realizable unitaries, and thus their presence cannot be detected.

On the other hand, perhaps surprisingly, it has been recently shown that in the presence of symmetries, this no-go theorem can be violated [3]. That is, 3-body interactions have certain signatures that are protected by the symmetry of the time evolution and cannot be reproduced by 2-body interactions. Based on this observation, Ref.[3] proposes a method for detecting the locality of interactions. However, as explained below, this method requires probing the unknown unitary V in the entire Hilbert space, rendering it inefficient for large systems.

In this article, we introduce a new symmetry-protected signature of 3-body interactions, denoted by the phase Δ_3 , and develop a method for efficient measurement of this quantity. Furthermore, we perform an experiment that measures this quantity on trapped atomic ion qubits, directly detecting the presence of 3-body interactions. A key component of our scheme, which enables efficient detection of 3-body interactions is the use of Greenberger–Horne–Zeilinger (GHZ) states [15]. Hence, our work reveals a novel application of GHZ states in the context of quantum sensing and Hamiltonian learning.

MAIN RESULTS

An observable phase protected by symmetry– Consider n qubits evolving under Hamiltonian $H(t)$ from time $t = 0$ to $t = T$. Assume the Hamiltonian respects the U(1) symmetry corresponding to rotations around the z -axis, or equivalently, it commutes with $\sum_j Z_j$. The unitary time evolution V generated under this Hamiltonian can then be decomposed as

$$V = \mathcal{T} \left\{ \exp \left(-i \int_0^T H(t) dt \right) \right\} = \bigoplus_{m=0}^n V_m, \quad (2)$$

where V_m is the component of the unitary V in the subspace with m “excitations”, or the eigen-subspace of $\sum_j (\mathbb{I} - Z_j)/2$ with eigenvalue m (also, known as the subspace with the Hamming weight m). The U(1) symmetry implies that the number of excitations m is conserved under unitary V , which explains the above block-diagonal form. For any such unitary, we define the phase

$$\Delta_3 \equiv \theta_{n-1} - \theta_1 - (n-2) \times (\theta_n - \theta_0) \pmod{2\pi}, \quad (3)$$

where

$$\theta_m \equiv \arg[\det(V_m)] \in (-\pi, \pi]$$

is the phase of the determinant of unitary V_m . Note that since $m = 0, n$ sectors are one-dimensional, $\theta_0 = \arg(V_0)$ and $\theta_n = \arg(V_n)$.

As we prove in Methods, the phase Δ_3 has the following properties: First, if the U(1)-invariant Hamiltonian $H(t)$ only contains 2-qubit interactions, then Δ_3 is an integer multiple of 2π . Therefore, $\Delta_3 \not\equiv 0 \pmod{2\pi}$ indicates the presence of interactions that couple more than 2 qubits together. In particular, for Hamiltonian $H^{(3)}$ in Eq.(1), assuming the two-body interactions in Hamiltonian $H^{(2)}$ are U(1)-invariant, we show that

$$\Delta_3 = -8 \int_0^T dt \sum_{i < j < k} a_{ijk}^{(3)}(t) \equiv -8\alpha_3 \pmod{2\pi}, \quad (4)$$

where we have defined the phase $\alpha_3 = \int_0^T dt \sum a_{ijk}^{(3)}(t)$. By measuring the phase Δ_3 and assuming the coefficients $a_{ijk}^{(3)}$ are time-independent, we can measure the net 3-body term $\sum a_{ijk}^{(3)}$, up to an integer multiple of $\pi(4T)^{-1}$. Hence, we can uniquely determine $\sum a_{ijk}^{(3)}$ either by measuring Δ_3 for a sufficiently short time T , or, alternatively, by measuring the phase Δ_3 for a few different values of time T . Also, if the interactions are translationally or permutationally invariant, this allows us to determine $a_{ijk}^{(3)}$.

Beyond this example, for a general U(1)-invariant Hamiltonian $H(t)$ in the Supplementay Material we establish the following remarkable identity:

$$\Delta_3 = -\frac{4}{2^n} \sum_{l \text{ odd}} (l-1) \int_0^T dt \text{Tr}[H(t)C_l] \pmod{2\pi}. \quad (5)$$

Here, the summation is over odd integers and for $l = 1, \dots, n$, the operator $C_l = \sum_{i_1 < i_2 < \dots < i_l} Z_{i_1} \dots Z_{i_l}$, where the summation is over $i_1, \dots, i_l \in \{1, \dots, n\}$ satisfying $i_1 < i_2 < \dots < i_l$. It follows that by adding the k -body interaction $a_{i_1, \dots, i_k}^{(k)}(t) Z_{i_1} \dots Z_{i_k}$ acting on k distinct qubits i_1, \dots, i_k to the Hamiltonian $H(t)$, the phase Δ_3 remains unchanged for even k , whereas for odd k it changes linearly as

$$\Delta_3 \longrightarrow \Delta_3 - 4(k-1) \int_0^T dt a_{i_1, \dots, i_k}^{(k)}(t) \pmod{2\pi}.$$

This, in particular, implies Eq.(4). It is also worth noting that the phase Δ_3 is additive in time. That is, by repeating the unitary V sequentially r times, which realizes the unitary V^r , the corresponding phase transforms as $\Delta_3 \rightarrow r\Delta_3$, which can be useful for amplifying this phase if 3-body interactions are weak.

It is interesting to compare this approach with the original

¹ For instance, for $n = 3$ and $n = 4$ qubits operator $C_3 = Z_1 Z_2 Z_3$ and $C_3 = Z_1 Z_2 Z_3 + Z_1 Z_2 Z_4 + Z_1 Z_3 Z_4 + Z_2 Z_3 Z_4$, respectively.

proposed scheme [3] based on the notion of l -body phases

$$\Phi_l \equiv - \int_0^T dt \operatorname{Tr}[H(t)C_l] = \sum_{m=0}^n c_l(m)\theta_m \pmod{2\pi}, \quad (6)$$

where integer $c_l(m) = \sum_{s=0}^l (-1)^s \binom{m}{s} \binom{n-m}{l-s}$ is the eigenvalue of C_l in the sector with m excitations. Note that while each l -body phase depends on all $\theta_m : m = 0, \dots, n$, and therefore its measurement requires probing the unitary V in an exponentially large Hilbert space, to determine Δ_3 , one only needs to probe the system in the $2(n+1)$ -dimensional subspace corresponding to the sectors with $m = 0, 1, n-1$, and n excitations. However, this extra exponential cost of measuring l -body phases comes with additional information about the locality of interactions: Φ_l is only sensitive to l -body interactions, i.e., unless $l = k$, by adding the k -body interaction $a_{i_1, \dots, i_k}^{(k)}(t) Z_{i_1} \dots Z_{i_k}$ to the Hamiltonian, the l -body phase Φ_l remains unchanged. It is also worth noting that in the special case of Hamiltonians in the form of Eq.(1) that only contain up to 3-body interactions, comparing Eq.(5) and Eq.(6), we find $\Phi_3 = 2^{n-3} \Delta_3 : \pmod{2\pi}$.

The measurement scheme—Next, we introduce a method for measuring the phase Δ_3 . Each phase θ_m is not observable individually, because it transforms non-trivially under the global phase transformation $V \rightarrow e^{i\phi} V$. To overcome this and find an efficient way of measuring Δ_3 , we rewrite Eq.(3) as

$$\Delta_3 = (\theta_{n-1} - n\theta_n) - (\theta_1 - n\theta_0) + 2(\theta_n - \theta_0) \pmod{2\pi}. \quad (7)$$

Now each of the three phases $\theta_n - \theta_0$, $\theta_1 - n\theta_0$, and $\theta_{n-1} - n\theta_n$ remains invariant under the above global phase transformation and can be experimentally measured as we demonstrate below.

First, $\theta_n - \theta_0$ is the relative phase between the fully occupied state $|1\rangle^{\otimes n}$ and the vacuum state $|0\rangle^{\otimes n}$. Thanks to the ability to prepare the GHZ state

$$|\text{GHZ}\rangle = \frac{|0\rangle^{\otimes n} + |1\rangle^{\otimes n}}{\sqrt{2}},$$

which is the equal superposition of these two states, this phase is directly observable via the standard phase sensing methods. Namely, by running the circuit (a) of Fig. 2, we measure the probability

$$|\langle \text{GHZ} | e^{iZ_1 \gamma/2} V | \text{GHZ} \rangle|^2 = \frac{1 + \cos(\theta_n - \theta_0 - \gamma)}{2}, \quad (8)$$

for a few different values of γ , which uniquely determines the phase $\theta_n - \theta_0 \pmod{2\pi}$.

Next, consider the phase $\theta_1 - n\theta_0 = \arg[\det(V_1)] - n\theta_0$, which can be interpreted as the total phases obtained by n single-excitation states relative to the vacuum state $|\mathbf{0}\rangle = |0\rangle^{\otimes n}$. Of course, standard process tomography allows the determination of V_1 , up to a global phase. However, in this way, we will not be able to detect the desired relative phase

because sensing that phase requires the interference between the 0 and 1 excitation states. To achieve this, we use the circuit (b) in Fig. 2 to measure the probability

$$|\langle \mathbf{0} | W_r e^{iZ_r \gamma/2} V W_s | \mathbf{0} \rangle|^2 = \frac{1 + A_{rs}^2 + 2A_{rs} \cos(\alpha_{rs} - \gamma)}{4}, \quad (9)$$

where $|\mathbf{0}\rangle = |0\rangle^{\otimes n}$ and W_s denotes the Hadamard gate on qubit s . Here, A_{rs} (α_{rs}) are the absolute value (phase) of the matrix element

$$[\tilde{V}_1]_{rs} = e^{-i\theta_0} \langle 1_r | V | 1_s \rangle \equiv A_{rs} e^{i\alpha_{rs}}, \quad (10)$$

for $r, s : 1, \dots, n$, where $|1_r\rangle = |0\rangle^{\otimes(r-1)} |1\rangle |0\rangle^{\otimes(n-r)}$ is the state with a single excitation at qubit r . Hence, by repeating this measurement for a few different values of γ , we can determine n^2 matrix elements $[\tilde{V}_1]_{rs}$. The determinant of this $n \times n$ matrix determines the phase $\theta_1 - n\theta_0 = \arg \det(\tilde{V}_1)$.

Finally, the phase $\theta_{n-1} - n\theta_n$, which can be interpreted as the total phase obtained by the single-hole states relative to the fully occupied state $|1\rangle^{\otimes n}$, can be measured in a similar fashion using the circuit in Fig. 2b, except in this case all qubits should be initialized in state $|1\rangle$. Combining these three phases using Eq.(7), we find the value of Δ_3 , via $\mathcal{O}(n^2)$ different measurement settings.

The experiment—We perform the experiment on 5 qubits within a 7-ion programmable trapped ion quantum computer, with all-to-all connectivity, individual addressing, and efficient state readout of all qubits [16–18] (see Methods for more details). In particular, we use hyperfine qubits of $^{171}\text{Yb}^+$ ions, with single-qubit gate fidelity of 99.6(2)% and two-qubit gate fidelity ranges from 99.3(1)% to 98.7(2)% for the qubit pairs used in this work (the fidelities are *not* corrected for state preparation and measurement [SPAM] errors estimated to be about 0.3%).

The ions are arranged in a linear chain, equidistantly spaced, and individually addressed with tightly focused beams passing through a multi-channel AOM, as depicted in the schematic of Fig. 3. The geometry of the individual addressing beams is perpendicular to the plane of the ion chain, enabling the addressing of transverse modes. With such capability, the system can implement universal gates for any qubit or pair of qubits. The native two-qubit gates are Mølmer-Sørensen or Ising operations between arbitrary pairs of qubits [19].

We employ automated calibration of single- or two-qubit gates and execute the large number of circuits required in the experiment with a periodic evaluation of the system's performance. Namely, we utilize a software-hardware API [20] alongside an automated calibration procedure within the hardware coding environment. This API optimizes and transpiles gate-level circuits into pulse sequences, then submits these sequences to an integrated hardware control system - ARTIQ (Advanced Real-Time Infrastructure for Quantum Physics) [21]. ARTIQ manages the coordination of the hardware system to execute the pulse sequences and

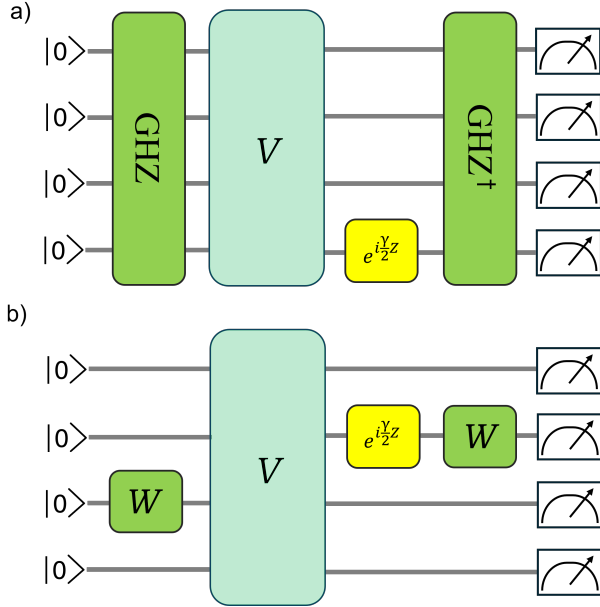


FIG. 2. **Circuits for measuring the phase Δ_3** : a) Measurement of $\theta_n - \theta_0$, or the phase between the fully occupied state $|1\rangle = |1\rangle^{\otimes n}$ and the vacuum $|0\rangle = |0\rangle^{\otimes n}$. The circuit first initializes the qubits in state $|0\rangle$ and prepares $|\text{GHZ}\rangle$ (e.g., through a Hadamard gate on the first qubit followed by a sequence of $n - 1$ CNOTs controlled by the first qubit). Next, an unknown unitary V is applied, followed by a single-qubit phase shift $e^{iZ\gamma/2}$ on one of the qubits, then a reversal of the GHZ generation and measurement of the qubits in the computational basis. The probability that all qubits are found in state $|0\rangle$ is given in Eq.(8). b) Measurement of $\theta_1 - n\theta_0 = \arg(\det(V_1)) - n\theta_0$, which can be interpreted as the total phase that single excitation states obtain with respect to the vacuum state. This circuit first initializes qubits in state $|0\rangle$, then applies a Hadamard gate W on qubit s , followed by unitary V and a single-qubit phase shift $e^{iZ\gamma/2}$ on qubit r , a single-qubit Hadamard W on qubit r , and finally measurement of the qubits in the computational basis. The probability of finding all qubits in state $|0\rangle$ is given by Eq.(9).

performs auto-calibrations as needed. By adhering to a software-hardware co-design principle, we enhance circuit execution efficiency and resilience to hardware interruptions, facilitating the handling of a large number of circuits with high performance.

Measuring Δ_3 – To demonstrate this method we utilize a setup with four qubits on a trapped-ion quantum simulator (See Fig. 4). In addition to one- and two-qubit $U(1)$ -invariant unitaries, the unknown unitary V also contains the three-qubit unitary $\exp(-i\alpha_3 Z_0 Z_1 Z_2)$ for $\alpha_3 \in (-\pi, \pi]$. The two-qubit gates exchange excitations between qubits, which means the realized $U(1)$ -invariant unitary is not diagonal in the computational basis. The phase Δ_3 for this circuit can be calculated from Eq.(1) to be $\Delta_3 = -8 \int_0^T dt \sum a_{ijk}^{(3)}(t) = -8\alpha_3$ (Note that any circuit can be interpreted as a time-dependent Hamiltonian evolution).

Then, to experimentally measure Δ_3 , we measure the three phases in Eq.(7) using the circuits in Fig. 2. The plot

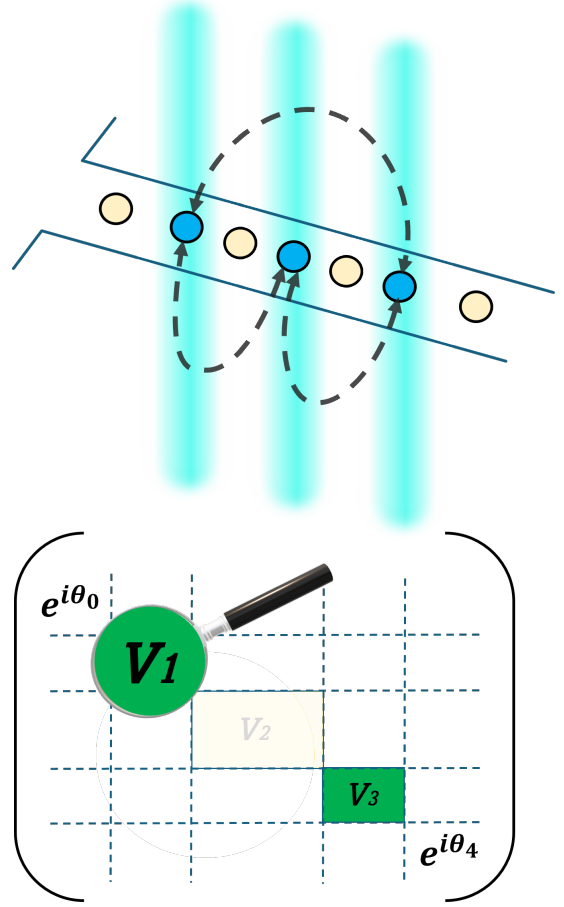


FIG. 3. **Schematic presentation of the experiment and the structure of $U(1)$ -invariant unitaries.** We introduce and experimentally demonstrate a novel method for detecting 3-body interactions. As shown in the top figure, we implement circuits with 4 and 5 trapped-ion qubits in a linear chain of 7 ions in an RF surface trap. Due to the individual addressing and all-to-all connectivity capabilities, we can execute single-qubit gates on any selected qubits and two-qubit gates on any chosen pair of qubits. The bottom figure represents a schematic depiction of a $U(1)$ -invariant unitary V on $n = 4$ qubits. To detect the presence of 3-body interactions, one only needs to probe the subspaces with $m = 0, 1, n - 1, n$ excitations. Specifically for $n = 4$ qubits, we do not need to probe the 6-dimensional subspace, with $m = 2$ excitations.

in Fig. 4 compares the outcome of the experiment with the theoretical prediction in Eq.(4). This plot clearly shows a distinctive feature of Δ_3 : it oscillates eight times faster than α_3 . Remarkably, for measuring the phase Δ_3 we do not need to probe the 6D subspace with $m = 2$ excitations. We also check that the phase Δ_3 does not change by varying 1-qubit and 2-qubit $U(1)$ -invariant gates (see Methods).

Additivity of Δ_3 – Another crucial feature of the phase Δ_3 is additivity: according to Eq.(4) all 3-body interactions have equal contributions in the phase Δ_3 . To experimentally verify this we consider the unitary V in the following form changed

$$V = S_2 e^{-i\zeta_2 Z_1 Z_2 Z_3} e^{-i\zeta_1 Z_0 Z_1 Z_2} S_1, \quad (11)$$

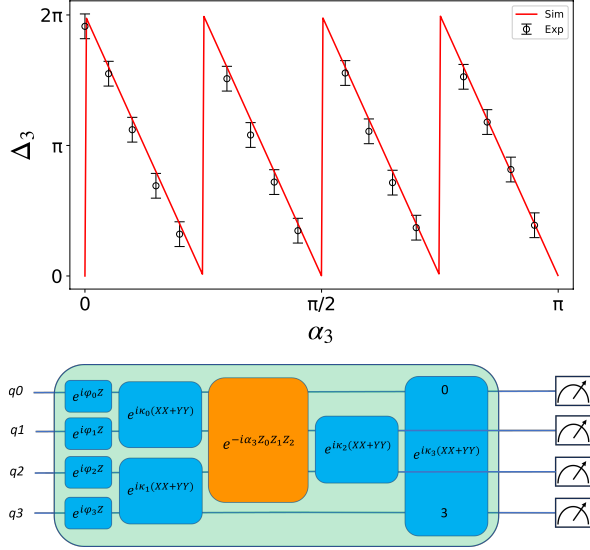


FIG. 4. **Measurement of the phase Δ_3 .** We perform measurement of Δ_3 for the U(1)-invariant unitary realized by the bottom circuit. Except for the unitary $\exp(-i\alpha_3 Z_0 Z_1 Z_2)$, the rest of the gates in this circuit are 1- and 2-qubit U(1)-invariant gates. The 2-qubit gates redistribute the excitations in the system. The plot compares the result of the experiment with the theoretical prediction of Eq.(4). As predicted, by varying the phase α_3 from 0 to π , Δ_3 oscillates four times. Angles $\varphi_0, \varphi_1, \varphi_2$, and φ_3 are $-\pi/5, \pi/16, 3\pi/16$, and $5\pi/14$, whereas $\kappa_0, \kappa_1, \kappa_2$, and κ_3 are $-\pi/14, -\pi/5, \pi/6$, and $\pi/9$. The error bars represent two standard deviations (2σ) determined by the bootstrap method (See Methods for further details).

on a system with $n = 4$ qubits, where S_1 , and S_2 are random 2-local U(1)-invariant unitaries, namely $\exp(i\phi Z_j)$, and $\exp(i\phi[X_j X_k + Y_j Y_k])$ for random values of ϕ . As it is shown in Fig. 5, by varying the 3-body interaction strength ζ_1 and ζ_2 , we experimentally verify the additivity of the phase Δ_3 . Specifically, we demonstrate that $\Delta_3 = -8(\zeta_1 + \zeta_2) \pmod{2\pi}$, which follows from Eq.(4).

Measuring l -body phases– In the last experimental setup, we measure the l -body phases in Eq.(6), which unlike Δ_3 allows us to distinguish k -body interactions, with different k . However, this requires performing full tomography by probing all sectors of unitary V .

In this experiment, we consider a system with $n = 4$ qubits evolving under the unitary

$$V = e^{-i\alpha_4 Z_0 Z_1 Z_2 Z_3} e^{-i\alpha_3 Z_1 Z_2 Z_3} S_2 S_1,$$

where S_1 and S_2 are random one- and two-qubit U(1)-invariant unitaries. To simplify the experiment and presentation, rather than varying α_3 and α_4 independently, we choose a particular ratio, namely $\alpha_3 = \alpha_4/3$. This can be interpreted as the unitary corresponding to the Hamiltonian $Z_0 Z_1 Z_2 Z_3 + \frac{1}{3} Z_1 Z_2 Z_3$ plus one- and two-qubit U(1)-invariant terms. Fig. 6 presents the corresponding 3-body and 4-body phases, Φ_3 and Φ_4 . As expected from Eq.(6), both Φ_4 and Φ_3 oscillate $2^n = 16$ times faster than α_4 and α_3 ,

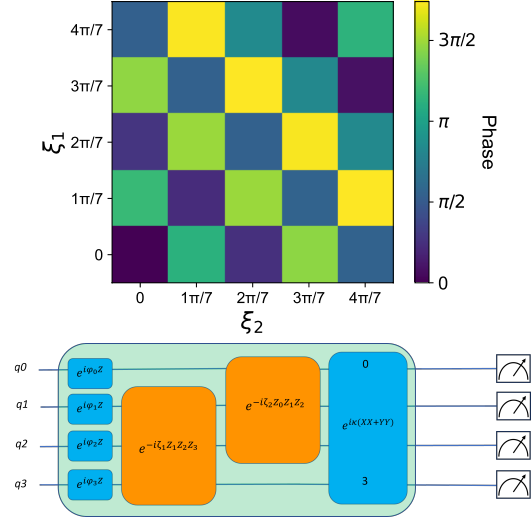


FIG. 5. **Experimental verification of the additivity of phase Δ_3 .** The circuit contains two 3-qubit gates $\exp(-i\zeta_1 Z_1 Z_2 Z_3)$ and $\exp(-i\zeta_2 Z_0 Z_1 Z_2)$. As predicted by Eq.(4), the phase Δ_3 is $-8(\xi_1 + \xi_2) \pmod{2\pi}$, which is consistent with the off-diagonal pattern in this plot. In this experiment, we set single-body z-rotation angles $\varphi_0, \varphi_1, \varphi_2$, and φ_3 to be $\pi/5, \pi/16, \pi/3$, and $\pi/12$, whereas θ is $-3\pi/10$ for two-qubit unitary. The error for each measured Δ_3 is ± 0.2 determined by the bootstrap method (See Methods for further details).

respectively.

To perform the process tomography on V , we use a technique that takes advantage of the U(1) symmetry of this unitary. On a system with n qubits, this symmetry implies that, instead of 4^n real parameters, to specify the unitary we need to determine $\sum_{m=0}^n \binom{n}{m}^2 = \binom{2n}{n} \approx 4^n / \sqrt{\pi n}$ [22] (For the present experiment this means $\binom{8}{4} = 70$ real numbers instead of $4^4 = 256$). Therefore, to take advantage of the symmetry constraints, rather than the standard tomography protocols which ignore this structure, we utilize a different technique. Namely, we use variants of the circuit (b) in Fig. 2, with more Hadamard gates at the input and output, which allows the creation of more excitations.

DISCUSSION

We introduced a new method for observing the symmetry-protected signature of 3-body interactions and performed the first-ever experiment demonstrating its measurement, enabling the direct detection of 3-body interactions. Our experiment was conducted on a trapped ion QC with an average 2-qubit gate error of 1%. The possibility of such direct detection of 3-body interactions was recently revealed in [3]. While the original method proposed in [3] requires full process tomography, the new scheme introduced in this paper only probes a subspace that scales linearly with the number of qubits. To achieve this, we take advantage of

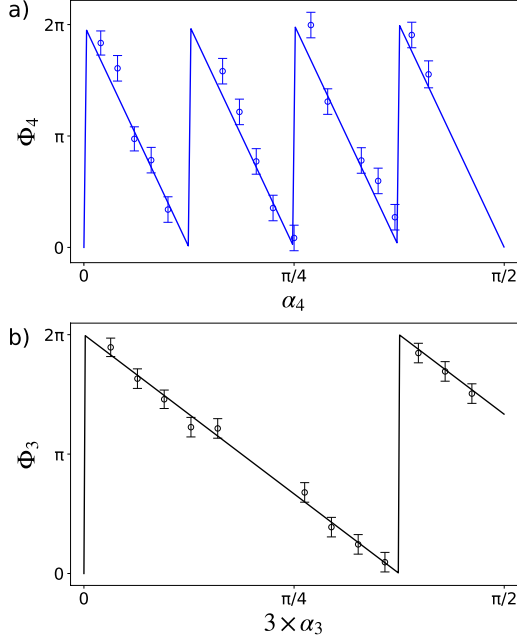


FIG. 6. **Measurement of 3-body and 4-body phases Φ_3 and Φ_4 .** In this experiment we measure Φ_3 and Φ_4 defined in Eq.(6), on $n = 4$ qubits for the unitary realized by the circuit in Fig. 12. To measure these quantities we have performed the full process tomography for this unitary. The circuit contains 4-qubit unitary $\exp(-i\alpha_4 Z_0 Z_1 Z_2 Z_3)$ and the 3-qubit unitary $\exp(-i\alpha_3 Z_1 Z_2 Z_3 Z_4)$, where for convenience in this circuit we have selected them such that $\alpha_4 = 3\alpha_3$ (i.e., we assume the 3-body interaction is three times weaker than the 4-body interaction). Eq.(6) implies that $\Phi_3 = 2^4 \alpha_3$, and $\Phi_4 = 2^4 \alpha_4$, which correspond to the solid black and blue lines in the above plots. Dots represent experimentally measured phases. The error bars on the figure represent two standard deviations (2σ) determined by the bootstrap method.

GHZ states, which allow us to directly measure the relative phase between the vacuum and fully occupied states. Without GHZ states, the presence of 3-body interactions can still be detected, although the efficiency will generally be lower. For instance, in Methods, we introduce a different scheme that does not use GHZ states; however, it requires probing the system in the subspace with 1, 2, and 3 excitations, whose total dimension scales as n^3 . This alternative scheme can be useful when preparing GHZ states is challenging, e.g., when the excitations are massive.

METHODS

I. PATH-INDEPENDENT OBSERVABLE PHASES PROTECTED BY SYMMETRY

The phase Δ_3 introduced in Eq. (3) is an example of a general formalism introduced in Ref. [3] for constructing path-independent phases under symmetric Hamiltonians. In the following, first, we review this formalism and then study the properties of phase Δ_3 . Finally, in Sec. ID, we introduce another family of such phases, which provides an alternative approach for detecting 3-body interactions.

A. Review: The formalism of the symmetry-protected path-independent phases

Consider a system with n qubits with the total Hilbert space $(\mathbb{C}^2)^{\otimes n}$. Let Π_m be the projector to the eigen-subspace of $\sum_{j=0}^n Z_j$ with eigenvalue $n - 2m$, i.e., the subspace with m excitations. Suppose this system evolves under U(1)-invariant Hamiltonian $H(t) : 0 \leq t \leq T$, which realizes the unitary $V = \mathcal{T}\{\exp(-i \int_0^T dt H(t))\}$. Then, U(1) symmetry implies that $H(t)$ and V decompose as $\bigoplus_m H_m(t)$ and $\bigoplus_m V_m$, where H_m and V_m are components of H and V in the subspace with m excitations, respectively. Furthermore,

$$V_m = \mathcal{T} \left\{ \exp \left[-i \int_0^T H_m(t) dt \right] \right\} \quad (12a)$$

$$= \lim_{L \rightarrow \infty} \prod_{j=1}^L \exp \left(-\frac{iT}{L} H_m \left(\frac{Tj}{L} \right) \right). \quad (12b)$$

Next, recall that for any pair of operators A_1 and A_2 , $\det(e^{A_1} e^{A_2}) = e^{\text{Tr}(A_1) + \text{Tr}(A_2)}$, which implies

$$\det(V_m) = \exp \left(-i \int_0^T \text{Tr}(H(t) \Pi_m) dt \right). \quad (13)$$

Defining $\theta_m = \arg[\det(V_m)]$, i.e., the phase of $\det(V_m)$, we conclude that for any set of integers $\{c(m)\}$,

$$\Phi \equiv \sum_m c(m) \theta_m = - \int_0^T dt \text{Tr}[H(t) C] \pmod{2\pi}, \quad (14)$$

where $C = \sum_m c(m) \Pi_m$. Note that θ_m is defined only mod 2π . Therefore, the phase Φ is well-defined only when coefficients $c(m)$ are integers. The above argument, in particular, means that if Hamiltonians $H_1(t)$ and $H_2(t)$ generate the same unitary V , then

$$\int_0^T dt \text{Tr}[H_1(t) C] = \int_0^T dt \text{Tr}[H_2(t) C] \pmod{2\pi}. \quad (15)$$

If operator C is traceless then Φ remains invariant under a global phase transformation $V \rightarrow e^{i\alpha} V$ for any $\alpha \in [0, 2\pi)$. This can be seen, e.g., using the fact that if Hamiltonian $H(t) :$

$0 \leq t \leq T$ realizes V , then Hamiltonian $H(t) - \frac{\alpha}{T}I : 0 \leq t \leq T$ realizes $e^{i\alpha}V$. For traceless operator C , $\text{Tr}(H(t)C)$ remains invariant under this transformation. Then, the second equality in Eq.(14) implies that the phase Φ remains invariant.

In summary, for any traceless operator $C = \sum_m c(m)\Pi_m$ with integer eigenvalues $\{c(m)\}$, the phase Φ defined in Eq.(14) is an observable quantity. As we see next, by measuring this phase we can obtain information about the locality of the Hamiltonian $H(t)$.

As an example, recall the definition of operators $\{C_l\}$ in [3]: Operator $C_0 = I^{\otimes n}$ is defined to be the identity operator on n qubits, and for $l = 1, \dots, n$

$$C_l = \sum_{i_1 < i_2 < \dots < i_l} Z_{i_1} \dots Z_{i_l}, \quad (16)$$

where the summation is over $i_1, \dots, i_l \in \{1, \dots, n\}$ that satisfy $i_1 < i_2, \dots, < i_l$. Operators C_l decomposes as

$$C_l = \sum_{m=0}^n c_l(m)\Pi_m, \quad (17)$$

where eigenvalues

$$c_l(m) = \sum_{s=0}^l (-1)^s \binom{m}{s} \binom{n-m}{l-s} \quad : m = 0, \dots, n, \quad (18)$$

are all integers [3]. Ref.[3] defines the l -body phase Φ_l associated to the time evolution generated by the U(1)-invariant Hamiltonian $H(t)$, as

$$\Phi_l \equiv - \int_0^T dt \text{Tr}[H(t)C_l] = \sum_{m=0}^n c_l(m)\theta_m \pmod{2\pi}, \quad (19)$$

where $\theta_m = \arg(\det(V_m))$. As explained before, by adding the k -body interaction $a_{i_1, \dots, i_k}^{(k)}(t)Z_{i_1} \dots Z_{i_k}$ acting on k distinct qubits i_1, \dots, i_k to the Hamiltonian $H(t)$, Φ_l remains unchanged for all l , except $l = k$. Therefore, by measuring Φ_l we can detect l -body interactions. See also [5] for the extension of this formalism to the case of SU(2) symmetry.

B. Localization in frequency and spatial domains

The above property of operators $\{C_l\}$ and the corresponding phases $\{\Phi_l\}$ means that they provide sharp information about the locality of interactions. However, because for each integer l the corresponding integers $\{c_l(m)\}$ are typically non-zero, to measure l -body phase Φ_l , we need to probe the entire Hilbert space, i.e., sectors with arbitrary excitation numbers $m = 0, \dots, n$.

The operators $\{C_l : l = 0, \dots, n\}$ and projectors $\{\Pi_m : m = 0, \dots, n\}$ are two different orthogonal bases, with respect to the Hilbert-Schmidt inner product, for the same oper-

ator space. That is, $\text{span}\{C_l\}_l = \text{span}\{\Pi_m\}_m$, and

$$\text{Tr}(C_l C_{l'}) = \delta_{l,l'} \times \text{Tr}(C_l^2) = \delta_{l,l'} \times 2^n \binom{n}{l}$$

and

$$\text{Tr}(\Pi_m \Pi_{m'}) = \delta_{m,m'} \times \text{Tr}(\Pi_m) = \delta_{m,m'} \times \binom{n}{m},$$

for all $l, l', m, m' = 0, \dots, n$. Hence, Eq.(17) describes a change of basis from one orthogonal basis to another. Furthermore, while the basis $\{C_l\}$ defines a sharp notion of locality, the basis $\{\Pi_m\}$ defines a sharp notion of the number of excitations (charge, or Hamming weight) in the system. The fact that integers $\{c_l(m)\}$ are typically non-zero, means that each element of the $\{C_l\}$ basis has support on many elements of the basis $\{\Pi_m\}$. In this sense, the transformation defined by Eq.(17) is analogous to the Fourier transform, and the relation between $\{\Pi_m\}$ and $\{C_l\}$ bases is analogous to the Fourier uncertainty relation.

As we explain next, from this point of view the phase Δ_3 , and the phases β_k defined in Sec.ID, correspond to operators that are partially localized in both spatial and frequency (charge) domains (See Fig. 7).

C. Δ_3 as a path-independent phase

Suppose in Eq.(14), we choose C to be the operator

$$F_3 = (n-2)(\Pi_0 - \Pi_n) - (\Pi_1 - \Pi_{n-1}), \quad (20)$$

which has integer eigenvalues and is traceless. Then, applying Eq.(14) we find that

$$\begin{aligned} \Delta_3 &= - \int_0^T dt \text{Tr}[H(t)F_3] \\ &= (n-2) \times (\theta_0 - \theta_n) - (\theta_1 - \theta_{n-1}) \pmod{2\pi}. \end{aligned} \quad (21)$$

To understand properties of the phase Δ_3 , in Appendix A we find the decomposition of operator F_3 in terms of $\{C_l\}$ operators. Namely, we show that

$$F_3 = -\frac{4}{2^n} \sum_{l:\text{odd}} (l-1)C_l, \quad (22)$$

where the summation is over odd integers in the interval $l = 1, \dots, n$ (See the middle part of Fig. 7 for a schematic representation of this equation). Putting this into Eq.(21) immediately implies Eq.(5). Furthermore, in the special case of Hamiltonians that can be decomposed as a sum of 3-body interactions, such as Hamiltonian $H^{(3)}(t)$ in Eq.(1), we have $\text{Tr}(C_l H_{2\text{-loc}}) = 0$ for $l > 2$. Moreover, for distinct i, j, k ,

$$\text{Tr}(C_l Z_i Z_j Z_k) = 2^n \delta_{3,l}.$$

This implies that for the time evolution under Hamiltonian in

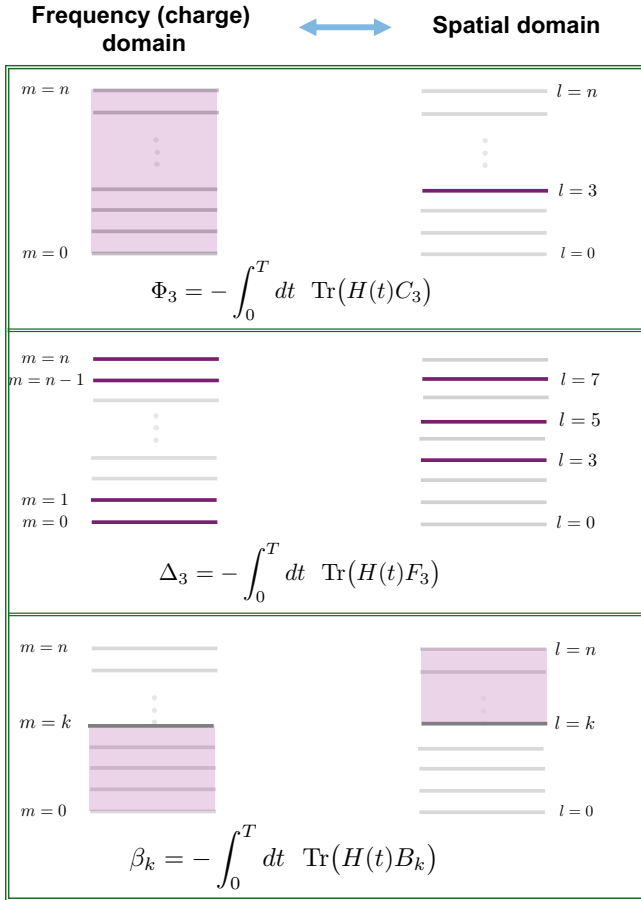


FIG. 7. **Frequency versus spatial domains**—The representation of operators C_3 defined in Eq.(16), F_3 defined in Eq.(20), and $\{B_k\}$ defined in Eq.(25), in the $\{\Pi_m\}$ basis (left) and $\{C_l\}$ basis (right). See the discussion in Sec.IB.

Eq.(1), we have

$$\Delta_3 = -8 \int_0^T dt \sum_{i < j < k} a_{ijk}^{(3)}(t) \pmod{2\pi},$$

which proves Eq.(4). In this case

$$\Phi_3 = 2^{n-3} \times \Delta_3 \pmod{2\pi}, \quad (23)$$

which can be obtained by comparing Eq.(5) with Eq.(6).

D. An alternative approach for detecting 3-body interactions

As we saw before, to measure the phase Δ_3 one needs to probe the subspaces with $m = 0, 1, n-1, n$ excitations. We saw that this can be achieved efficiently, provided that one can prepare GHZ states that contain superposition of states with $m = 0$ and $m = n$ excitations. However, for some applications, preparing such a superposition might be unfeasible (e.g., when the excitations are massive).

For such applications, here we introduce another family of

path-independent phases, which can be measured by probing the system in the sectors with $m = 0, 1, 2, 3$ excitations. Indeed, we introduce a more general formalism that allows us to detect k -body interactions by probing the sectors with $m = 0, \dots, k$ excitations.

For $k \leq n$, define the phase

$$\begin{aligned} \beta_k &\equiv \sum_{m=0}^k (-1)^m \binom{n-m}{k-m} \theta_m \\ &= -\int_0^T dt \text{Tr}(B_k H(t)) \pmod{2\pi}, \end{aligned} \quad (24)$$

where operator

$$B_k = \sum_{m=0}^k (-1)^m \binom{n-m}{k-m} \Pi_m. \quad (25)$$

This definition, in particular, means that operators $\{B_k\}$ are linearly independent, and form a basis for the operator space

$$\text{span}\{\Pi_m\} = \text{span}\{C_l\} = \text{span}\{B_k\}. \quad (26)$$

Note that β_k only depends on $\theta_0, \dots, \theta_k$. For instance, for $k = 3$, we find

$$\beta_3 = \binom{n}{3} \theta_0 - \binom{n-1}{2} \theta_1 + (n-2) \theta_2 - \theta_3 \pmod{2\pi}.$$

For the special case of $n = 3$ qubits, we have

$$n = 3 : \quad B_3 = F_3 = C_3 = Z^{\otimes 3}, \quad (27)$$

which implies $\beta_3 = \Delta_3 = \Phi_3$.

The crucial property of operators $\{B_k\}$, which is proven in the Supplementary Material, is the following: For all $k, l = 0, \dots, n$ we have

$$\text{Tr}(B_k C_l) = 0 \quad : l < k \quad (28a)$$

$$\text{Tr}(B_k C_k) = 2^{k-n} \times \text{Tr}(C_k^2) = 2^k \binom{n}{k}. \quad (28b)$$

The bottom part of Fig. 7 presents a schematic representation of Eq.(28) and Eq.(25). In particular, except $k = 0$, which corresponds to $B_0 = |0\rangle\langle 0|^{\otimes n}$, the rest of operators $\{B_k\}$ are traceless, which means $\beta_k : k = 1, \dots, n$ are experimentally observable. Note that according to Eq.(24), to measure β_k , we only need to probe sectors with $m = 0, \dots, k$ excitations.

Furthermore, applying this equation, in Appendix B, we show that

Lemma 1. *Suppose operator H can be written as a sum of k -local terms. Then,*

$$\text{Tr}(HB_k) = \frac{2^k \times \text{Tr}(HC_k)}{2^n}, \quad (29)$$

and $\text{Tr}(HB_r) = 0$ for $r > k$.

This lemma implies that for U(1)-invariant Hamiltonian H

in the form of Eq.(1),

$$\beta_3 = \Delta_3 = -8 \int_0^T dt \sum_{i < j < k} a_{ijk}^{(3)}(t) \pmod{2\pi}. \quad (30)$$

More generally, consider the Hamiltonian

$$H(t) = H_{(k-1)\text{-loc}}(t) + \sum_{j_1 < \dots < j_k} a_{j_1 \dots j_k}^{(k)}(t) Z_{j_1} Z_{j_2} \dots Z_{j_k}, \quad (31)$$

where $H_{(k-1)\text{-loc}}(t)$ is an unknown U(1)-invariant Hamiltonians that does not contain k -body interactions, i.e., can be decomposed as the sum of $(k-1)$ -local U(1)-invariant terms. For this Hamiltonian, we obtain

$$\beta_k = -2^k \int_0^T dt \sum_{j_1 < \dots < j_k} a_{j_1 \dots j_k}^{(k)}(t) \pmod{2\pi}. \quad (32)$$

FURTHER DETAILS AND ERROR ANALYSIS FOR THE EXPERIMENT

Trapped Ion Quantum Computer: We decompose the transverse modes of seven $^{171}\text{Yb}^+$ ions and estimate the effect of noise and drifts on the gates [23]. This analysis is followed by constructing segmented optical pulses tailored for the entangling gates to ensure their robustness. Gate duration and pulse shaping are adjusted for individual ion pairs to minimize coupling to motion at the end of the gate pulse sequence.

The two-qubit gates fidelity measurement technique is outlined in [17]. A single-qubit gate is a composite SK1 pulse [24]. For SPAM measurement, we prepare qubits in the $|0\rangle$ (dark) and $|1\rangle$ (bright) states, then perform a Poisson fit to the histograms corresponding to these two states. The resulting SPAM is 0.27(4)%.

Circuit Design and Optimization: For all circuits, commuting single-qubit rotations and two-qubit $\text{XX}(\pi/4)$ gates are merged to minimize the circuit size. However, while the unitary operator V is still subject to optimization, its content is not merged with the external circuit elements and is treated as a ‘black box’. The 3-body and 4-body unitaries $\exp(-i\alpha_3 Z_0 Z_1 Z_2)$ and $\exp(-i\alpha_4 Z_0 Z_1 Z_2 Z_3)$ are realized using standard methods for implementing Pauli Hamiltonians, via a sequence of CNOTs [25].

Post-Processing and Statistical Error: Data presented in the main text are the result of several post-processing steps. First, we extract the population from the raw histograms for different values of γ . Then we perform fitting to extract observable phases. The next step is a construction of the total phases corresponding to 3- or 4-body interaction following Eq.(3) or Eq.(6), respectively.

Fig. 8 demonstrates the outcomes of the phase estimation experiment for measuring $\theta_4 - \theta_0$, with 4-qubit GHZ state. Specifically, we measure the population at $|0000\rangle$ for two distinct interaction strengths of the 3-body interaction, $\alpha_3 = \pi/5$ and $\alpha_3 = 9\pi/10$. For each interaction strength, we vary γ (see Eq.(8)), then we perform fitting with a sinusoidal function to

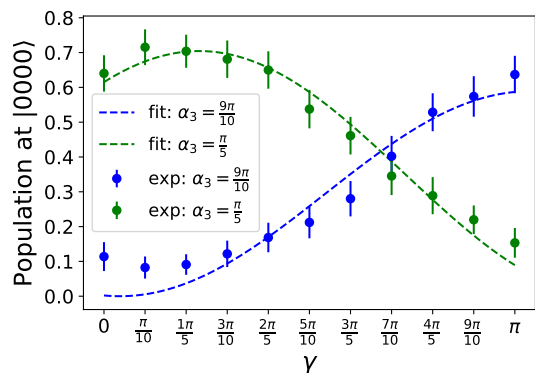


FIG. 8. **Phase estimation using 4-qubit GHZ state** Using the circuit in Fig. 4, we measure the phase $\theta_4 - \theta_0$ via Eq. (8). We present two setups corresponding to three-qubit unitaries $\exp(-i\alpha_3 Z_0 Z_1 Z_2)$ with $\alpha_3 = \pi/5$ and $\alpha_3 = 9\pi/10$. For each value of interaction strength α_3 , we vary γ in Eq.(8). By fitting the resulting curves with sinusoidal functions, we extract the phase offsets corresponding to the phase $\theta_4 - \theta_0$. See the caption of Fig. 4 for further details on the realized unitary V in this experiment. The error bars represent two standard deviations (2σ) determined by the bootstrapping method discussed below.

obtain the contrasts and ensure the correct measurement of the phase offset. According to Eq.(8), the measured phase offset determines the phase $\theta_4 - \theta_1$ (A similar technique is used to determine the phase $\alpha_{r,s}$ via Eq.(9)). In this particular example, we measure $\theta_4 - \theta_0$ referenced in Eq.(8). We use a similar procedure followed by Eq.(9) to measure the rest of the observable phases.

We use a statistical bootstrapping method [26] to estimate uncertainties by 1000 expectation values with each value evaluated based on a 150-shot histogram randomly resampled from the original 300-shot readout. The error bars indicate 2σ from the bootstrap distribution.

Noise Model: We examine hardware error sources by directly measuring errors and simulating hardware output using the Qiskit platform [27]. We describe a two-qubit gate error in the z - and x -bases. For all ion pairs used in this work, the errors measured in the z -basis are in the range from 0.28(5)% to 0.85(4)%, whereas errors in the x -basis are in the range from 0.01(1)% to 0.04(1)%. The dominant noise in this model is incoherent (Pauli) error.

We compare output histograms to noiseless theoretical histograms, all corresponding to 300 shots. As an illustrative example, we select an experiment employing GHZ state on 4 qubits, which is often considered as the most sensitive state to noise. In Fig. 9, parts (a) and (b) correspond to two different experiments, where in (a) $\alpha = 0.02\pi$ and $\gamma = \pi$, and in (b) $\alpha = 0.165\pi$ and $\gamma = 2\pi/5$. To simplify the presentation, we consider probabilities only for states $|0000\rangle$ and $|0001\rangle$, which are the only states with non-zero probability in the absence of noise (In Fig. 9 this is illustrated as ‘Theory, noiseless’).

We introduce independent single-qubit Pauli errors, according to the above noise model. The results are depicted in Fig. 9 as ‘Theory, noisy’. We apply the same error model across

all qubits, assuming errors within experimentally measured ranges. With the considered noise model, one can see a good match between noisy theoretical prediction (Fig. 9, ‘Theory, noisy’) and experimental results (Fig. 9, ‘Experiment’). We compute the 1-norm of the probability vector space difference between the experiment and noisy simulation to demonstrate the agreement for the rest of the binary state subspace. The measured values do not exceed 0.05.

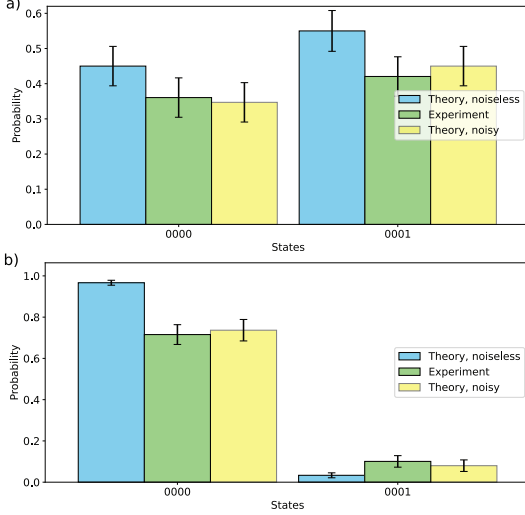


FIG. 9. **Error model evaluation.** Outcome of GHZ experiment/simulation on 4 qubits with (a) $\alpha = 0.02\pi$ and $\gamma = \pi$, and (b) $\alpha = 0.165\pi$ and $\gamma = 2\pi/5$. For clarity, only $|0000\rangle$ and $|0001\rangle$ states are presented. All histograms depict output data with 300 shots. The ‘Theory, noisy’ histogram is compared to the ‘Experiment’ histogram to assess the noise model. The error bars on the figure represent two standard deviations (2σ) determined by the bootstrapping method discussed below.

GHZ parity benchmark: We conduct a GHZ interference experiment to evaluate the performance of our system. When utilizing GHZ states, errors in individual qubits have a cascading effect, impacting the overall performance. Hence, such experiments provide a powerful method for benchmarking the system. Fig. 10 (b) presents a schematic of the circuit employed for these measurements, and Fig. 10 (a) displays the corresponding GHZ parity fringe observed across four qubits. We perform regular system calibrations to achieve this contrast level throughout the experiment.

Insensitivity of Δ_3 with respect to 1- and 2- body Interactions: In Fig. 11 we present the outcome of a 3-qubit experiment to verify that Δ_3 is indeed independent of one- and two-body interactions. The horizontal axis ϕ determines the phase of a single-qubit gate $\exp(-i\phi Z_0)$ and two-qubit

$\exp(-i\frac{\phi}{2}(X_0X_1 + Y_0Y_1))$. We check that while the three phases $\theta_3 - \theta_1$, $\theta_1 - 3\theta_0$ and $\theta_2 - 3\theta_3$ all vary non-trivially with ϕ , as expected from our theoretical results, the phase $\Delta_3 = \theta_{n-1} - \theta_1 - (n-2) \times (\theta_n - \theta_0)$ does not depend on ϕ .

Circuits for Φ_3 and Φ_4 measurement: In Fig. 6 we presented the results of measuring the phases Φ_3 and Φ_4 for the 4-qubit unitary realized by the circuit in Fig. 12. As expected from

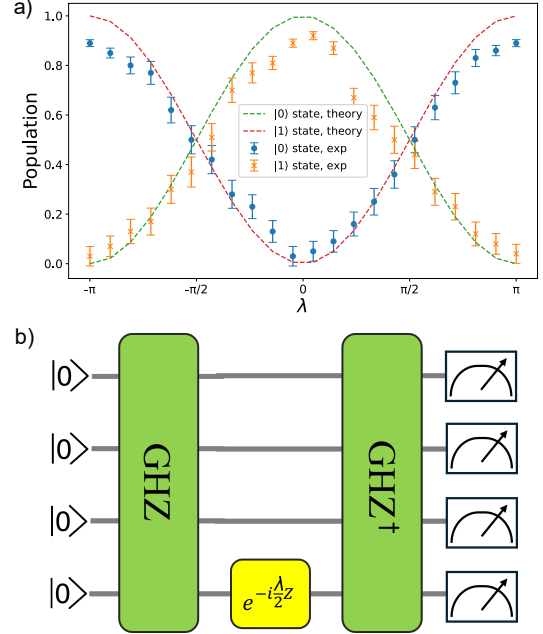


FIG. 10. **GHZ parity fringe benchmarking on four qubits.** a) GHZ parity fringe for the subset of four qubits in a seven-ion linear chain. We use the notation $|0\rangle = |0\rangle^{\otimes 4}$ and $|1\rangle = |1\rangle^{\otimes 4}$. ‘Theory’ curves represent parity fringe without noise or statistical error. The error bars on the figure represent two standard deviations (2σ) determined by the bootstrapping method discussed below. b) Schematic circuit for GHZ parity measurement. We vary the phase λ to observe a parity fringe.

Eq.(6), we observe that varying single- and two-qubit gates do not affect the measured Φ_3 or Φ_4 phases.

ACKNOWLEDGEMENTS

This work is supported by the DOE Quantum Systems Accelerator (DE-FOA-0002253), the NSF STAQ Program (PHY-1818914), the NSF QLCI grant OMA-2120757, the Army Research Office (W911NF-21-1-0005), as well as NSF grants Phy-2046195 and FET-2106448.

- [1] O. Katz, M. Cetina, and C. Monroe, Programmable n-body interactions with trapped ions, PRX Quantum **4**, 030311 (2023).
 [2] O. Katz, L. Feng, A. Risinger, C. Monroe, and M. Cetina, Demonstration of three- and four-body interactions between

- trapped-ion spins, Nature Physics **19**, 1452 (2023).
 [3] I. Marvian, Restrictions on realizable unitary operations imposed by symmetry and locality, Nature Physics **18**, 283 (2022).

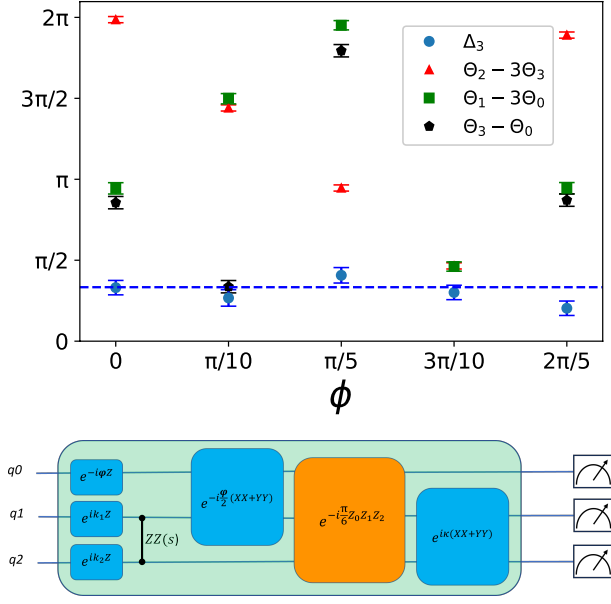


FIG. 11. **Independence of Δ_3 from one- and two-body interactions.** For the unitary realized in the bottom circuit, we measure the phase Δ_3 . The horizontal axis is ϕ that determines the phase of a one- and two-qubit gates in the circuit. While all three phases $\theta_2 - 3\theta_3$ (red), $\theta_1 - 3\theta_0$ (green), $\theta_3 - \theta_0$ vary non-trivially with ϕ , as predicted by our theory, the resulting total phase Δ_3 (blue) remains approximately unchanged and consistent with the theoretical prediction of Eq.(4), namely $\Delta_3 = -8\alpha_3 = \pi/3 \pmod{2\pi}$, within the error margins. The gate $ZZ(s)$ denotes $\exp(-i\frac{s}{2}Z \otimes Z)$. In this experiment, $k_1 = \pi/16$, $k_2 = 3\pi/16$, $s = 4\pi/5$, $\kappa = \pi/6$.

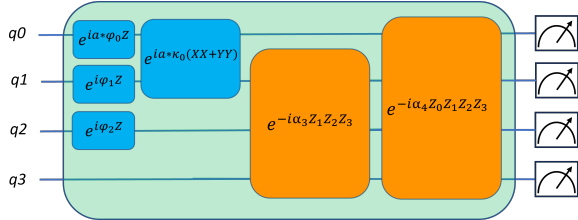


FIG. 12. **Circuits and corresponding parameters for Φ_3 and Φ_4 measurement.** In this circuit, the single-body z -rotation angles φ_0 , φ_1 , and φ_2 are respectively $-\pi/10$, $\pi/16$, $3\pi/16$, and a is in the range from 0 to 10. The result of the measurement of Φ_3 and Φ_4 is presented in Fig. 6.

[4] Á. M. Alhambra, Forbidden by symmetry, *Nature Physics* **18**, 235 (2022).
 [5] I. Marvian, H. Liu, and A. Hulse, Rotationally invariant circuits: Universality with the exchange interaction and two ancilla qubits, *Physical Review Letters* **132**, 130201 (2024).
 [6] V. Giovannetti, S. Lloyd, and L. Maccone, Quantum-enhanced measurements: Beating the standard quantum limit, **306**, 1330 (2004).
 [7] V. Giovannetti, S. Lloyd, and L. Maccone, Advances in quantum metrology, *Nature Photonics* **5**, 222 (2011).

[8] C. L. Degen, F. Reinhard, and P. Cappellaro, Quantum sensing, *Reviews of modern physics* **89**, 035002 (2017).
 [9] H.-Y. Huang, Y. Tong, D. Fang, and Y. Su, Learning many-body hamiltonians with heisenberg-limited scaling, *Physical Review Letters* **130**, 200403 (2023).
 [10] H.-W. Hammer, A. Nogga, and A. Schwenk, Colloquium: Three-body forces: From cold atoms to nuclei, *Reviews of modern physics* **85**, 197 (2013).
 [11] M. e. Tse, H. Yu, N. Kijbunchoo, A. Fernandez-Galiana, P. Dupej, L. Barsotti, C. Blair, D. Brown, S. Dwyer, A. Effler, *et al.*, Quantum-enhanced advanced ligo detectors in the era of gravitational-wave astronomy, *Physical Review Letters* **123**, 231107 (2019).
 [12] F. Acernese, M. Agathos, L. Aiello, A. Allocca, A. Amato, S. Ansoldi, S. Antier, M. Arène, N. Arnaud, S. Ascenzi, *et al.*, Increasing the astrophysical reach of the advanced virgo detector via the application of squeezed vacuum states of light, *Physical review letters* **123**, 231108 (2019).
 [13] D. P. DiVincenzo, Two-bit gates are universal for quantum computation, *Physical Review A* **51**, 1015 (1995).
 [14] S. Lloyd, Almost any quantum logic gate is universal, *Physical Review Letters* **75**, 346 (1995).
 [15] D. M. Greenberger, M. A. Horne, and A. Zeilinger, Going beyond bell's theorem, in *Bell's theorem, quantum theory and conceptions of the universe* (Springer, 1989) pp. 69–72.
 [16] Y. Nam, J. Chen, N. Piseni, and *et al.*, Ground-state energy estimation of the water molecule on a trapped-ion quantum computer, *npj Quantum Information* **6**, 10.1038/s41534-020-0259-3 (2020).
 [17] L. Egan, D. Debroy, C. Noel, and *et al.*, Fault-tolerant control of an error-corrected qubit, *Nature* **598**, 10.1038/s41586-021-03928-y (2021).
 [18] M. Cetina, L. Egan, C. Noel, M. Goldman, D. Biswas, A. Risinger, D. Zhu, and C. Monroe, Control of transverse motion for quantum gates on individually addressed atomic qubits, *PRX Quantum* **3**, 010334 (2022).
 [19] A. Sørensen and K. Mølmer, Quantum Computation with Ions in Thermal Motion, *Phys. Rev. Lett.* **82**, 1971 (1999).
 [20] Q. Wang, L. Zhukas, Q. Miao, A. S. Dalvi, P. J. Love, C. Monroe, F. T. Chong, and G. S. Ravi, Demonstration of a cafqbootstrapped variational quantum eigensolver on a trapped-ion quantum computer, *arXiv preprint arXiv:2408.06482* (2024).
 [21] S. Bourdeauducq, R. Jördens, P. Zotov, J. Britton, D. Slichter, D. Leibbrandt, D. Allcock, A. Hankin, F. Kermarrec, Y. Sionneau, R. Srinivas, T. R. Tan, and J. Bohnet, *Artiq* **1.0** (2016).
 [22] G. Bai and I. Marvian, Synthesis of energy-conserving quantum circuits with xy interaction, *arXiv preprint arXiv:2309.11051* (2023).
 [23] Y. Wu, S.-T. Wang, and L.-M. Duan, Noise analysis for high-fidelity quantum entangling gates in an anharmonic linear paul trap, *Phys. Rev. A* **97**, 062325 (2018).
 [24] K. R. Brown, A. W. Harrow, and I. L. Chuang, Arbitrarily accurate composite pulse sequences, *Phys. Rev. A* **70**, 052318 (2004).
 [25] M. Nielsen, Universal quantum computation using only projective measurement, quantum memory, and preparation of the 0 state (2001), [quant-ph/0108020](https://arxiv.org/abs/quant-ph/0108020).
 [26] B. Efron and R. Tibshirani, *An Introduction to the Bootstrap* (Chapman and Hall/CRC, New York, 1994).
 [27] A. Javadi-Abhari, M. Treinish, K. Krsulich, C. J. Wood, J. Lishman, J. Gacon, S. Martiel, P. D. Nation, L. S. Bishop, A. W. Cross, B. R. Johnson, and J. M. Gambetta, *Quantum computing with Qiskit* (2024), [arXiv:2405.08810](https://arxiv.org/abs/2405.08810) [quant-ph].

Supplementary Material:

Observation of the symmetry-protected signature of 3-body interactions

Appendix A: Properties of phase Δ_3 (Proof of Eq.(5))

In this Appendix, we prove Eq.(5). To prove this equation it is useful to remember some properties of operators

$$C_l = \sum_{i_1 < i_2 < \dots < i_l} Z_{i_1} \cdots Z_{i_l} = \sum_{m=0}^n c_l(m) \Pi_m .$$

where the eigenvalues

$$c_l(m) = \sum_{s=0}^l (-1)^s \binom{m}{s} \binom{n-m}{l-s} \quad : m = 0, \dots, n, \quad (\text{A1})$$

are all integers. It can be easily seen that $X^{\otimes n} \Pi_m X^{\otimes n} = \Pi_{n-m}$, i.e., under applying Pauli X on all qubits the m -excitation sector is transformed to m -hole sector. Furthermore, since C_l is decomposed as a sum of tensor products of l Pauli Z operators, we find $X^{\otimes n} C_l X^{\otimes n} = (-1)^l C_l$. This, in particular, implies

$$c_l(m) = \frac{\text{Tr}(C_l \Pi_m)}{\text{Tr}(\Pi_m)} = \frac{\text{Tr}(X^{\otimes n} C_l \Pi_m X^{\otimes n})}{\text{Tr}(X^{\otimes n} \Pi_m X^{\otimes n})} = (-1)^l \frac{\text{Tr}(C_l \Pi_{n-m})}{\text{Tr}(\Pi_{n-m})} = (-1)^l \times c_l(n-m) . \quad (\text{A2})$$

Operators $C_l : l = 0, \dots, n$ are linearly independent and satisfy the orthogonality relation

$$\text{Tr}(C_l C_{l'}) = \delta_{l,l'} \times \text{Tr}(C_l^2) = 2^n \times \binom{n}{l} . \quad (\text{A3})$$

It follows that the subspace spanned by $\{\Pi_m : m = 0, \dots, n\}$ is equal to the subspace spanned by operators $\{C_l : l = 0, \dots, n\}$. This subspace has dimension $n+1$. This is indeed the subspace of operators that commute with U(1)-invariant Hamiltonians.

Any operator H has a decomposition as

$$H = H_{\perp} + \sum_{l=0}^n \frac{\text{Tr}(H C_l)}{\text{Tr}(C_l^2)} C_l , \quad (\text{A4})$$

with the property that

$$\text{Tr}(H_{\perp} \Pi_m) = \text{Tr}(H_{\perp} C_l) = 0 \quad : m, l = 0, \dots, n . \quad (\text{A5})$$

Applying this decomposition to operator $F_3 = (n-2)(\Pi_0 - \Pi_n) - (\Pi_1 - \Pi_{n-1})$, we find that

$$F_3 = \sum_{l=0}^n \frac{\text{Tr}(F_3 C_l)}{\text{Tr}(C_l^2)} C_l . \quad (\text{A6})$$

Using the facts that $X^{\otimes n} F_3 X^{\otimes n} = -F_3$ and $X^{\otimes n} C_l X^{\otimes n} = (-1)^l C_l$, we find that

$$\text{Tr}(F_3 C_l) = \text{Tr}([X^{\otimes n} F_3 X^{\otimes n}][X^{\otimes n} C_l X^{\otimes n}]) = -(-1)^l \text{Tr}(F_3 C_l) , \quad (\text{A7})$$

which implies $\text{Tr}(F_3 C_l) = 0$ for even l .

On the other hand, for odd l , Eq.(A2) we find

$$\text{Odd } l : \text{Tr}(F_3 C_l) = 2(n-2) \times c_l(0) - 2n \times c_l(1) . \quad (\text{A8})$$

Next, applying the formula for $c_l(m)$ in Eq.(A1) we find

$$\text{Tr}(F_3 C_l) = 2(n-2) \binom{n}{l} - 2n \binom{n-1}{l} + 2n \binom{n-1}{l-1} \quad (\text{A9})$$

$$= 2 \left[(n-2) \frac{n!}{(n-l)! \times l!} - n \frac{(n-1)!}{(n-l-1)! \times l!} + n \frac{(n-1)!}{(n-l)! \times (l-1)!} \right] \quad (\text{A10})$$

$$= \frac{2 \times (n-1)!}{(n-l-1)! \times l!} \times \left(\frac{n(n-2) + nl}{n-l} - n \right) \quad (\text{A11})$$

$$= \frac{2 \times (n-1)!}{(n-l-1)! \times l!} \times \left(\frac{2n \times (l-1)}{n-l} \right) \quad (\text{A12})$$

$$= 4(l-1) \times \binom{n}{l}. \quad (\text{A13})$$

Putting this in Eq.(A6) we find

$$F_3 = \sum_{l=0}^n \frac{\text{Tr}(F_3 C_l)}{\text{Tr}(C_l^2)} C_l = \sum_{l:\text{odd}} 4(l-1) \times \binom{n}{l} \frac{1}{2^n \times \binom{n}{l}} C_l = \frac{4}{2^n} \sum_{l:\text{odd}} (l-1) C_l. \quad (\text{A14})$$

This implies that

$$\Delta_3 = - \int_0^T dt \text{Tr}[H(t) F_3] \quad (\text{A15})$$

$$= (n-2) \times (\theta_0 - \theta_n) - (\theta_1 - \theta_{n-1}) \quad (\text{A16})$$

$$= -\frac{4}{2^n} \sum_{l:\text{odd}} (l-1) \int_0^T dt \text{Tr}[H(t) C_l] \pmod{2\pi},$$

and completes the proof of Eq.(5).

Appendix B: An alternative approach for detecting 3-body interactions (Properties of phase β_k and operator B_k)

We prove that for all $l, r \leq n$, it holds that

$$\sum_{l=0}^n \text{Tr}(B_r C_l) \times (i \tan \theta)^l = \binom{n}{r} (2i)^r \frac{e^{i\theta(n-r)}}{(\cos \theta)^{n-r}} \times (\tan \theta)^r \quad : -\pi < \theta \leq \pi. \quad (\text{B1})$$

The proof is presented at the end of this section. For $\theta = 0$, the left-hand side of this equation becomes

$$\text{Tr}(B_r) = \binom{n}{r} (2i)^r \delta_{r,0} = \delta_{r,0}, \quad (\text{B2})$$

which means except $B_0 = |0\rangle\langle 0|^{\otimes n}$ the rest of $\{B_r\}$ are traceless.

For $|\theta| \ll 1$, the right-hand side of Eq.(B1) is equal to

$$\binom{n}{r} (2i)^r \times \theta^r + \mathcal{O}(\theta^{r+1}). \quad (\text{B3})$$

The left-hand side, on the other hand, becomes

$$\text{Tr}(B_r C_{l_{\min}}) \times (i\theta)^{l_{\min}} + \mathcal{O}(\theta^{l_{\min}+1}), \quad (\text{B4})$$

where l_{\min} is the smallest value of l for which $\text{Tr}(C_l B_r)$ is non-zero. Comparing the two sides, we can immediately see that

$$\text{Tr}(B_r C_l) = 0 \quad : l < r \quad (\text{B5a})$$

$$\text{Tr}(B_r C_r) = 2^r \binom{n}{r}. \quad (\text{B5b})$$

Next, using this identity we prove lemma 1.

It is also worth noting that by taking derivatives with respect to θ of both sides of Eq.(B1), at $\theta = 0$, this equation implies

$$\text{Tr}(B_r C_l) = \frac{(-i)^l (2i)^r}{l!} \binom{n}{r} \times \frac{d^l}{d\theta^l} \left[e^{i\theta(n-r)} \frac{(\sin \theta)^r}{(\cos \theta)^n} \right]_{\theta=0}. \quad (\text{B6})$$

1. Proof of lemma 1

First, using Eq.(A4) we find

$$\text{Tr}(B_r H) = \text{Tr}(B_r H_{\perp}) + \sum_{l=0}^n \text{Tr}(C_l B_r) \frac{\text{Tr}(C_l H)}{\text{Tr}(C_l^2)}. \quad (\text{B7})$$

Since B_r is a linear combination of $\{\Pi_m\}$ operators, Eq.(A5) implies $\text{Tr}(H_{\perp} B_r) = 0$. Therefore, we find

$$\text{Tr}(H B_r) = \sum_{l=0}^n \text{Tr}(C_l B_r) \frac{\text{Tr}(H C_l)}{\text{Tr}(C_l^2)} \quad (\text{B8})$$

$$= \sum_{l=0}^k \text{Tr}(C_l B_r) \frac{\text{Tr}(H C_l)}{\text{Tr}(C_l^2)}, \quad (\text{B9})$$

where to get the second line we have used the assumption that H can be written as a sum of k -local terms, and therefore it is orthogonal to operator C_l for $l > k$. Applying Eq.(B5), we find that for $r > k$, $\text{Tr}(H B_r) = 0$, and for $r = k$

$$\text{Tr}(H B_k) = \sum_{l=0}^k \text{Tr}(C_l B_k) \frac{\text{Tr}(H C_l)}{\text{Tr}(C_l^2)} \quad (\text{B10})$$

$$= \text{Tr}(C_k B_k) \frac{\text{Tr}(H C_k)}{\text{Tr}(C_k^2)} \quad (\text{B11})$$

$$= \frac{2^k \binom{n}{k}}{2^n \binom{n}{k}} \text{Tr}(H C_k) \quad (\text{B12})$$

$$= 2^{k-n} \times \text{Tr}(H C_k). \quad (\text{B13})$$

This proves lemma 1.

2. Proof of Eq.(B1)

First, using the Euler formula $e^{i\theta Z} = \cos \theta I + i \sin \theta Z$, we find

$$(e^{i\theta Z})^{\otimes n} = (\cos \theta I + i \sin \theta Z)^{\otimes n} = \sum_{l=0}^n (\cos \theta)^{n-l} (i \sin \theta)^l \sum_{j_1 < \dots < j_l} Z_{j_1} \cdots Z_{j_l} \quad (\text{B14})$$

$$= \sum_{l=0}^n (\cos \theta)^{n-l} (i \sin \theta)^l C_l \quad (\text{B15})$$

$$= (\cos \theta)^n \sum_{l=0}^n (i \tan \theta)^l C_l. \quad (\text{B16})$$

This implies that

$$\text{Tr}((e^{i\theta Z})^{\otimes n} B_k) = \sum_{l=0}^n (\cos \theta)^{n-l} (i \sin \theta)^l \text{Tr}(B_k C_l). \quad (\text{B17})$$

Next, we use the fact that

$$(e^{i\theta Z})^{\otimes n} = \sum_{m=0}^n e^{i\theta(n-2m)} \Pi_m, \quad (\text{B18})$$

and

$$\text{Tr}(\Pi_m) = \binom{n}{m}. \quad (\text{B19})$$

This implies

$$\text{Tr}(B_k (e^{i\theta Z})^{\otimes n}) = \sum_{m=0}^k (-1)^m \frac{(n-m)!}{(n-k)!(k-m)!} \times \frac{n!}{(n-m)!m!} e^{i\theta(n-2m)} \quad (\text{B20})$$

$$= \frac{n!}{(n-k)!} \sum_{m=0}^k (-1)^m \frac{1}{m!(k-m)!} e^{i\theta(n-2m)} \quad (\text{B21})$$

$$= \frac{n! e^{i\theta n}}{(n-k)!k!} \sum_{m=0}^k (-1)^m \frac{k!}{m!(k-m)!} e^{-i\theta 2m} \quad (\text{B22})$$

$$= e^{i\theta n} \binom{n}{k} \sum_{m=0}^k (-1)^m \binom{k}{m} e^{-i\theta 2m} \quad (\text{B23})$$

$$= \binom{n}{k} e^{i\theta n} \times (1 - e^{-i2\theta})^k. \quad (\text{B24})$$

In summary, we found

$$\text{Tr}(B_k (e^{i\theta Z})^{\otimes n}) = \binom{n}{k} e^{i\theta n} \times (1 - e^{-i2\theta})^k \quad (\text{B25})$$

$$= \binom{n}{k} e^{i\theta(n-k)} \times (e^{i\theta} - e^{-i\theta})^k \quad (\text{B26})$$

$$= \binom{n}{k} (2i)^k e^{i\theta(n-k)} \times (\sin \theta)^k. \quad (\text{B27})$$

Comparing this with Eq.(B17), we find

$$(\cos \theta)^n \sum_{l=0}^n (i \tan \theta)^l \text{Tr}(B_k C_l) = \binom{n}{k} (2i)^k e^{i\theta(n-k)} \times (\sin \theta)^k, \quad (\text{B28})$$

or, equivalently,

$$\sum_{l=0}^n (i \tan \theta)^l \text{Tr}(B_k C_l) = \binom{n}{k} (2i)^k \frac{e^{i\theta(n-k)}}{(\cos \theta)^{n-k}} \times (\tan \theta)^k. \quad (\text{B29})$$